LANGMUIR

pubs.acs.org/Langmuir Article

Oxidative Spin-Spray-Assembled Coordinative Multilayers as Platforms for Capacitive Films

Mikko Salomäki,* Lauri Marttila, Henri Kivelä, Matti Tupala, and Jukka Lukkari*

Cite This: *Langmuir* 2020, 36, 6736–6748

Read Online

ACCESS | Metrics & More | Article Recommendations | Supporting Information

ABSTRACT: The spin-spray-assisted layer-by-layer (LbL) assembly technique was used to prepare coordinative oxidative multilayers from Ce(IV), inorganic polyphosphate (PP), and graphene oxide (GO). The films consist of successive tetralayers and have a general structure $(PP/Ce/GO/Ce)_n$. Such oxidative multilayers have been shown to be a general platform for the electrodeless generation of conducting polymer and melanin-type films. Although the incorporation of GO enhances the film growth, the conventional dip LbL method is very time consuming. We show that the spin-spray method reduces the time required to grow thick multilayers by the order of magnitude and the film growth is linear from the beginning, which implies a stratified structure. We have deposited poly(3,4-ethylenedioxothiophene), PEDOT, on the oxidative multilayers and studied these redox-active films as models for melanin-type capacitive layers for supercapacitors to be used in biodegradable electronics, both before and after the electrochemical reduction of GO to rGO. The amount of oxidant and PEDOT scales linearly with the film thickness, and the charge transfer kinetics is not mass transfer-limited, especially after the reduction of GO. The areal capacitance of the films grows linearly with the film thickness, reaching a value of *ca.* 1.6 mF cm^{-2} with 20 tetralayers, and the specific volumetric (per film volume) and mass (per mass of PEDOT) capacitances are *ca.* 130 F cm^{-3} and 65 F g^{-1}, respectively. 5,6-Dihydroxyindole can also be polymerized to a redox-active melanin-type film on these oxidative multilayers, with even higher areal capacitance values.

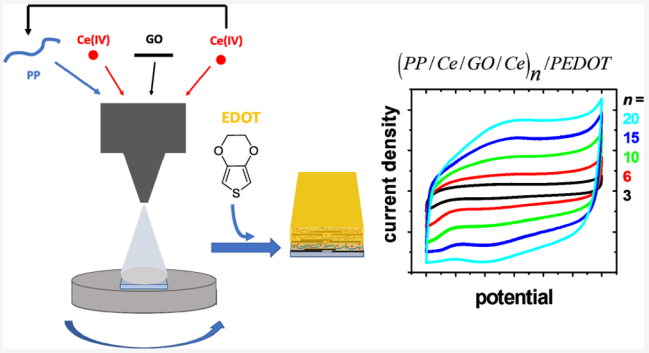

INTRODUCTION

A successive layer-by-layer (LbL) self-assembly of charged components is an extremely versatile technique for the fabrication of thin films with a wide variety of materials.[1] The oldest LbL technique involves dipping a substrate alternately in solutions of oppositely charged polyions (dip LbL), but spin, spray, and spin-spray-assisted LbL techniques have shown great promise. In most cases, the individual layers are bound together by Coulombic interactions, but coordinative bonding and hydrogen bonding can also be used to prepare LbL multilayers. However, despite the widespread use of this technique, only a few noncatalytic chemically reactive LbL multilayers have been described in the literature.[2,3] We have demonstrated that an oxidative multilayer based on coordinative bonding between a redox-active transition metal, for example, Ce(IV), and a polyanion, for example, inorganic polyphosphate (PP), can be used as a general platform to generate thin conducting polymer or polydopamine films on surfaces.[4−6] Incorporation of graphene oxide (GO) sheets into the multilayer greatly enhances its growth and allows it to bind a larger amount of oxidant in the multilayer, resulting in thicker polymer films.[7]

Redox-active polymer films can be used as pseudocapacitive components in supercapacitors. In general, supercapacitors have many advantageous properties in energy storage.[8] They exhibit long cycle life and high power density because of fast charge and discharge rates. Simple electrochemical double-layer capacitors (EDLCs) have a low energy density, which can be increased using high-surface-area carbon materials.[9] In EDLCs, the energy is stored electrostatically within the electrical double layer at the electrode−solution interface, but faradaic reactions can be used to increase the storage capacity. In pseudocapacitors, the energy is stored in the oxidation state of the electroactive materials. The fast redox reaction between the substrate electrode and the electroactive material is accompanied by ion flux in and out of the surface film. The highest storage density can be achieved in hybrid systems, which combine the high-surface-area EDLCs with effective pseudocapacitance. In general, the capacitance of

Received: March 24, 2020
Revised: May 12, 2020
Published: May 26, 2020

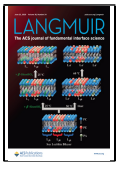

https://dx.doi.org/10.1021/acs.langmuir.0c00824
Langmuir 2020, 36, 6736−6748

supercapacitors varies in the range from some tens to hundreds of Faradays per gram (or cm^3) of the material.[8−10]

Metal oxides and conducting polymers are typical pseudocapacitive components in supercapacitors.[9] Conducting polymers are widely used because they are highly conductive, flexible, and easily prepared.[9−11] Among conducting polymers, polyaniline (PANI), polypyrrole (PPy), and various polythiophene derivatives, especially poly(3,4-ethylenedioxythiophene) (PEDOT), are the most commonly utilized pseudocapacitive materials. PEDOT, especially, has been extensively studied for supercapacitors because of its high conductivity, chemical, thermal, and electrochemical stability, and the facile preparation of thin films using the PEDOT:poly(styrene sulfonate) (PSS) mixture.[12,13]

The major disadvantage of pure conducting polymer-based electrode materials is the volumetric swelling and shrinking of the material during electrochemical cycles, which decreases their cycle life.[10] Pure PEDOT films possess the same general disadvantages as other conducting polymers, and it is usually combined with carbon nanotubes, GO, or metal oxides.[9,10] The capacitance values reported for PEDOT-based films vary greatly. The highest reported capacitance of pure PEDOT films is 300 F g^{-1}, but generally, the values obtained are much smaller.[14−23] With films prepared using the LbL self-assembly, GO is a convenient component as it is cheap, is easily prepared in large quantities, and can be incorporated into the multilayers because of its anionic charge and coordinative properties. Even though GO is electrically insulating, it can easily be reduced to a conductive form (reduced graphene oxide, rGO), which can improve the film conductivity. Hybrid films containing carbon nanotubes or graphene-based materials generally display specific capacitance values of around 100−200 F g^{-1}, but some values outside of this range have also been reported.[13,24−34] Still much higher capacitance values can be achieved if metal oxides are incorporated into the structure.[32,35−38] The wide spread of the reported values underlines the sensitivity of the measured film capacitance on its composition and structure and the fabrication and measurement techniques.

We have previously shown that GO enhances the mechanical properties of oxidative $(PP/Ce)_n$ multilayers formed by the dip LbL technique and that the formed $(PP/Ce/GO/Ce)_n$ films grow much faster, reaching a thickness of *ca.* 230 nm already after five (PP/Ce/GO/Ce) tetralayers.[4,7] In these films, Ce(IV) reversibly binds to the oxygen-containing groups of PP and GO with coordinative bonds, and the larger amount of Ce(IV) in these hybrid multilayers allows thicker conducting polymer films to be oxidized on them. However, the morphology of these dip LbL multilayers is not well defined and their surface roughness is very high. In this work, we have prepared oxidative (PP/Ce/GO/Ce) multilayer films using the automated, fast, and inexpensive spin-spray LbL film deposition technique, in which small volumes of reagent solutions are sequentially sprayed on the horizontally spinning substrate (Scheme 1).[39,40] The spin-spray LbL technique is a relatively new LbL technique, which combines many advantages of the spin LbL and spray LbL techniques.[39,41−45] With the spin-spray LbL technique, the individual layers are thinner than those with the dip LbL method but their deposition time is greatly shortened. The centrifugal force advances the draining and subsequent drying of the surface, and the assembly of an individual layer, including the rinsing and drying of the film, takes less than a minute. In addition, the

Scheme 1. Preparation of Oxidative Multilayers and Polymer Films Using the Spin-Spray LbL Technique and Postassembly Polymerization (PP = Inorganic Polyphosphate and GO = Graphene Oxide)

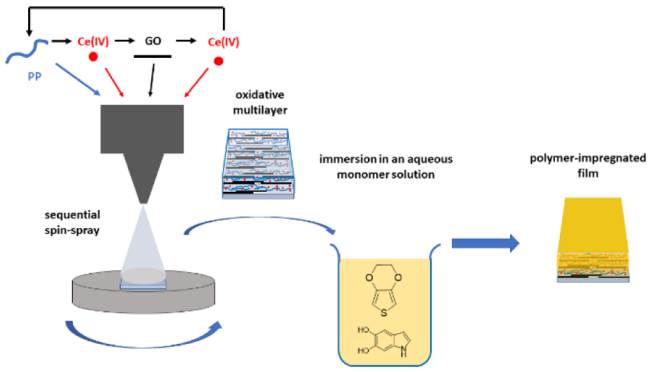

spin-spray technique requires less material and decreases the material waste, leading to smoother films with more uniform electrical and optical properties.[39,41,42,46,47] With the dip LbL technique, the multilayer build-up is exponential, at least in the beginning, but with the spin-spray method, the films grow linearly, they are generally more stratified, and the plate-like components are more parallel to the surface. The spin-spray LbL technique has been applied, for example, to conducting and transparent films,[46,48] gas barrier films,[47,49] antifogging coatings,[50] films for corrosion or electromagnetic shielding,[51,52] and in batteries.[46,48]

Although the dip LbL and spray LbL techniques have been compared previously,[44,53−56] there are only a few papers thoroughly comparing the spin-spray and dip LbL techniques.[46,47] The work mostly emphasizes the effect of the deposition method on the film morphology, thickness, and the material consumption. However, the chemically reactive (PP/Ce/GO/Ce) LbL multilayers set some specific requirements for the film properties, and it is necessary to see the effect of the LbL technique on intrafilm diffusion of the reactants (oxidant and monomers), the reactant capacity, the reaction kinetics, and the formation and properties of the produced post-LbL-assembly film. This is especially important because the gas permeation studies have shown that the spin-spray-assembled films with plate-like components are better barriers than those prepared using the dip LbL technique.[47,49] Therefore, the aim of this work is twofold. First, we study the effect of the deposition technique on the structure and properties of coordinative multilayers containing large plate-like GO particles. We compare the growth, morphology, oxidative capacity, reaction kinetics, and electrochemistry of the spin-spray LbL $(PP/Ce/GO/Ce)_n$ films, with and without PEDOT, to the previously studied dip LbL $(PP/Ce/GO/Ce)_n$ and $(PP/Ce)_n$ films. Second, we will demonstrate that the oxidative multilayers are promising general systems for the fabrication of thin polymer-based electroactive films with high specific capacitance. Layered supercapacitors have been prepared with conducting polymers using electropolymerization and similar techniques,[11] but there are only a few examples of the use of a true dip LbL[57,58] or spray LbL[59,60] technique. In these cases, prepolymerized polyaniline was used, although an aerogel with *in situ*-polymerized PEDOT sandwiched between metal oxide layers has also been reported.[61] However, this work demonstrates the use of a true spin-spray LbL technique and the *in situ* oxidative

https://dx.doi.org/10.1021/acs.langmuir.0c00824
Langmuir 2020, 36, 6736−6748

polymerization of any suitable monomer (the oxidation potential is the main limiting factor).[5] The electrochemical properties of the spin-spray LbL $(PP/Ce/GO/Ce)_n$/PEDOT films are studied with cyclic voltammetry and *in situ* ultraviolet−visible (UV−vis) spectroscopy as a function of the oxidative film thickness. In particular, we are interested in the specific areal, volumetric, and mass capacitance of the films as they can show the potential of such films for supercapacitor structures.

There are basically two different test configurations for supercapacitors, the two-electrode and three-electrode configurations.[62] In a two-electrode system, the films forming the capacitor are sandwiched together and separated by a thin porous film. This configuration is typical for the actual supercapacitor devices. The three-electrode configuration, on the other hand, is a typical setup for electrochemical studies, and it contains only one electrode (working electrode) covered by the active capacitive material. The capacitance values obtained from measurements with the two setups are not identical. In general, there is no direct functional dependence between the values except with symmetric capacitors, but the capacitances obtained by the three-electrode configuration are approximately twice those obtained by the other method. The two-electrode configuration measures the device capacitance, while the specific capacitance of the active material is given by the electrochemical setup. Therefore, when comparing the reported values, care should be taken to observe the configuration used. On the other hand, the three-electrode configuration is often used because it allows a fast and facile screening of materials and films and can offer important information about the processes taking place in the film, especially when using cyclic voltammetry.

Our final goal is to find materials and composite films for supercapacitors to be used for driving small biodegradable electronic devices. In fact, PEDOT may not be the best material for biodegradable systems, although it has good biocompatibility, but we use it here as an easily prepared model material to assess the applicability of oxidative films for supercapacitor fabrication.[63,64] However, we have previously shown that melanin-type films can also be prepared using oxidative films starting from 5,6-dihydroxyindole and that Ce(IV) is an efficient oxidant for the preparation of polydopamine from dopamine,[6,65] and we also present preliminary results of polydopamine-based capacitive films formed using the oxidative multilayers. This demonstrates the potential of using oxidative spin-spray LbL multilayers as general platforms for the facile and rapid production of capacitive films, also with biocompatible materials.

EXPERIMENTAL SECTION

Materials. Cerium(IV) ammonium nitrate (Sigma-Aldrich), sodium chloride (J.T. Baker), sodium sulfate (VWR), 3,4-ethylenedioxythiophene (EDOT, TCI), and *N*-trimethoxysilylpropyl-*N*,*N*,*N*-trimethylammonium chloride (TMSPA, 50% in methanol, ABCR) were used as received. Potassium metaphosphate (98%, ABCR) was washed with water several times using vacuum filtration with a Büchner funnel and dried at 110 °C in order to remove residual phosphoric acid from the reagent. Graphene oxide was prepared from natural graphite (Alfa Aesar, 325 mesh) using a downscaled version of the modified Hummers method[66] with a synthesis procedure that has been described before.[67] Water distilled twice in quartz vessels was used for the preparation of aqueous solutions.

Substrates. Films for atomic force microscopy (AFM) and light microscopy analysis and some scanning electron microscopy (SEM) samples were assembled on phosphorus-doped (100) silicon wafers (Okmetic, Finland). All other films were assembled on glass slides with a SnO_2 coating on one surface (Pilkington K glass) or on glass or quartz slides with indium tin oxide (ITO) coating on one surface (≤20 Ω/□). Silicon wafers were cleaned in a fresh Piranha solution (a 3:1 volume ratio of conc. H_2SO_4 and 30% H_2O_2. WARNING! Piranha solution is extremely corrosive and should not be stored in tightly closed vessels!) for at least 1 h, rinsed with water, and dried first with N_2 gas and then at 110 °C for at least 1 h. SnO_2- or ITO-coated slides were washed in a 5:1:1 volume ratio solution of H_2O, 25% ammonium hydroxide, and 30% H_2O_2 for 30 min, rinsed with water, and dried similarly to the silicon wafers.

LbL Assembly of Oxidative Films. 10 mM cerium(IV) ammonium nitrate, 10 mM polyphosphate solutions (PP, 10 mM KO_3P and 0.1 M NaCl, diluted by stirring overnight), and a 0.3 mg/mL GO suspension were used in the LbL assembly. Fresh PP solutions were always used in order to minimize polymer hydrolysis.[68] The GO suspension was exfoliated in an ultrasonic bath (VWR USC500THD) for 30 min before use. A 10 mM EDOT solution was prepared in H_2SO_4 (pH = 1.5) by ultrasonicating the mixture for 30 min (Hielscher UP100H). All substrates were silanized with 1:9 v/v TMSPA/methanol solution before the LbL assembly for 10 min, washed with methanol and water, and dried with N_2 gas in order to positively charge the surface. The LbL multilayer films were deposited using an automatized spin-spray multilayer deposition device, described in detail previously (Scheme 1).[40] Briefly, substrates were attached to a horizontal spinner below the air channel of the spraying unit, and the spinning speed was allowed to stabilize to 1500 ± 200 rpm. Pressurized air is constantly driven through the air channel above the substrate toward it. During the film assembly, solutions are flown one by one through the polyether ether ketone (PEEK) tube inside the air channel. The air flow breaks the liquid into a mist and sprays it on the substrate. The following spraying scheme was used for the $(PP/Ce/GO/Ce)_n$ multilayers: (1) reagent solution for 3 s followed by 20 s of drying and (2) rinsing with a water spray for 10 s, followed by 20 s of drying. These steps were repeated until a desired number of layers were deposited (before the assembly of each (PP/Ce/GO/Ce) tetralayer, an additional couple of seconds delay was required for instrumental reasons). After the process, films were further rinsed with water and/or dried if necessary, and the oxidative film on the nonconducting sides of the ITO-coated wafers was carefully removed using cotton sticks, ≥25% ammonium hydroxide solution, water, and N_2 gas for rinsing and drying.

Polymerization of EDOT and Polydopamine. EDOT was polymerized on the LbL films by immersing the oxidative films in 10 mM monomer solutions (an aqueous pH 1.5 H_2SO_4 solution) for 16−20 h within a few hours after oxidative film preparation (Scheme 1; the oxidative power of the films decreases with time[5]). Finally, films were rinsed with water and dried after polymerization. When required, the nonconductive side of the ITO slides was cleaned with cotton sticks and water in order to remove possible PEDOT coatings from the backside of the substrates. Polydopamine was polymerized onto the oxidative spin-spray LbL film similarly to that previously described by exposing the oxidative multilayer to a 5,6-dihydroxyindole solution for 100 min.[6]

Film Characterization. The PEDOT polymerization on the ITO-coated slides in the stirred EDOT monomer solutions was followed by UV−vis spectroscopy at 25 °C (Agilent Cary 60 with a constant-temperature cell holder). All other UV−vis spectra were measured with the Agilent Cary 60 or a HP 8453 Diode Array UV−vis spectrophotometer. The light microscopy pictures were taken with a Hysitron Ubi 1 nanomechanical test instrument (Hysitron, Inc.), and the SEM images were taken with a Thermo Scientific FEI Apreo S ultrahigh resolution field emission scanning electron microscope or a Jeol JSM-6335F scanning electron microscope. The AFM images were measured from the representative areas of the dry films on a silicon wafer at a controlled temperature and relative humidity with an AFM microscope (diCaliber, Bruker) using the tapping mode. The water content of the dry films was allowed to stabilize for at least 1 h before the AFM measurements. The thickness of the films was measured

https://dx.doi.org/10.1021/acs.langmuir.0c00824
Langmuir 2020, 36, 6736−6748

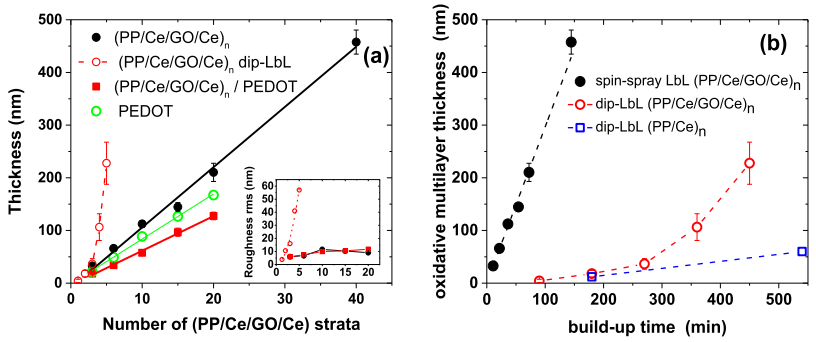

Figure 1. [7](a) Thickness of $(PP/Ce/GO/Ce)_n$ (solid black) and $(PP/Ce/GO/Ce)_n$/PEDOT (solid red) spin-spray-assembled films measured by AFM, effective thickness of the PEDOT film (open green circles) as a function of the number of tetralayers (n), and linear fits to the data; error bars represent standard deviations of multiple measurements. The inset shows the rms surface roughness of the films; given error bars represent standard deviations of multiple measurements (lines are only a guide to the eye). (b) Thickness of the oxidative multilayer as a function of the time required for the film build-up process. In (a) and (b), the behavior of dip LbL $(PP/Ce/GO/Ce)_n$ films is shown for comparison (open red circles).

with AFM by making a slit to the films with a scalpel. The image processing and analysis were carried out using Gwyddion 2.50 software. Thickness or the root-mean-square (rms) surface roughness of the films was estimated using the mean or combined mean values of the representative areas of the images. Error bars represent standard deviation or combined standard deviation of multiple measurements.

Electrochemical and spectroelectrochemical measurements were made using a computer-controlled potentiostat (Autolab PGSTAT101; IviumStat, Ivium Technologies or PalmSens4, PalmSens) in a three-electrode configuration. The $(PP/Ce/GO/Ce)_n$ or $(PP/Ce/GO/Ce)_n$/PEDOT films on ITO- or SnO_2-coated slides were used as a working electrode, the platinum wire was used as an auxiliary electrode, and the miniature Ag/AgCl electrode was used as a reference electrode. All potentials are given against this electrode (the potential of the electrode was checked before and after every measurement, and it deviated less than 10 mV from the Ag/AgCl (sat. KCl) reference electrode). The studied films were immersed into 0.5 M Na_2SO_4 electrolyte solution deaerated with nitrogen. The electrochemically active film area of the films (*ca.* 0.5−1.5 cm^2) was estimated by measuring the area of the immersed films.

RESULTS AND DISCUSSION

Growth and Structure of Spin-Sprayed Oxidative Multilayers. The LbL films consisting of successive tetralayers of (PP/Ce/GO/Ce) can be grown very fast using the spin-spray technique. The thickness of the spin-sprayed multilayers grows linearly from the beginning, contrary to the corresponding dip LbL films (Figure 1a). The latter exhibited exponential growth in the beginning, which is indicative of intrafilm diffusion during the assembly.[7,69] Exponential growth was observed also with (PP/Ce) multilayers prepared using the dip LbL technique.[4] The linear growth of the spin-sprayed films can be attributed to the high shear stress within the thin solution layer and its rapid drying, which shortens the time available for structural rearrangements or diffusion during the assembly process.[39,41,46,47] In addition, the GO sheets will also be aligned with the surface and diminish intrafilm diffusion. Linear growth is, in fact, generally observed with spin-sprayed polyelectrolyte multilayers.[42,46] The growth of the spin-sprayed film was found to be linear at least up to 40 tetralayers (maximum number of layers tested in this work), with an increase of 11 nm per one (PP/Ce/GO/Ce) tetralayer. As a function of the number of tetralayers, these films are considerably thinner than the corresponding multilayers prepared using the dip LbL technique and reach *ca.* 50 nm after five (PP/Ce/GO/Ce) strata, which is only *ca.* 20% of that of a dip LbL film with the same number of tetralayers.[7] From the practical point of view, a huge difference can be seen when the obtained multilayer thickness is plotted as a function of the build-up time (Figure 1b). The build-up time has been calculated based on the reported deposition schemes, assuming no additional breaks between the steps.[4−7] The spin-spray technique produces thinner individual layers, but the time required to reach a given total thickness is dramatically shorter than that with the traditional dip LbL technique. Introduction of GO sheets in the structure also greatly enhances the multilayer growth.

When the oxidative $(PP/Ce/GO/Ce)_n$ multilayers were immersed in dilute aqueous solutions of EDOT, a polymer film was formed on the surface. The thickness of the $(PP/Ce/GO/Ce)_n$/PEDOT films still scaled linearly with the number of oxidative (PP/Ce/GO/Ce) tetralayers (Figure 1a), but the average thickness per nominal (PP/Ce/GO/Ce) stratum is only *ca.* 7 nm. All these AFM-based thickness measurements have been carried out with dried films, and because Young's modulus of spin-casted and electrochemically polymerized PEDOT films is of the order of 1−2 GPa,[70] we tentatively attribute this shrinkage to the elastic properties of the drying polymer film filling the pores in the oxidative multilayer. This is analogous to the deformation of the adjacent layers in a photovoltaic device by the water-swollen PEDOT layer.[71] This conclusion is also supported by the spectroscopically estimated effective thickness of the deposited PEDOT film in contact with solution, shown also in Figure 1a (*vide infra*). The thickness of the PEDOT film is close to that of the dry oxidative multilayer, which implies that the polymer film penetrates the multilayer, filling the available pores and possibly restructuring the film, instead of forming only at the multilayer/solution interface. This is also supported by the high redox capacity of the polymer.

Overlapping GO sheets can be seen in the AFM and SEM images of the spin-sprayed oxidative $(PP/Ce/GO/Ce)_n$ multilayers, except with thick polymer films (Figures 2 and S1). On thick $(PP/Ce/GO/Ce)_n$/PEDOT films, a clear globular surface structure becomes apparent. The rms roughness (obtained from 10 μm × 10 μm AFM images) of both films increases up to 10 tetralayers (*ca.* 110 nm) but levels off with thicker films. The surface roughness is much smaller, both in absolute value and in relation to the film thickness, than that in the corresponding films prepared using the dip LbL technique but still higher than that in the $(PP/Ce)_n$ films

https://dx.doi.org/10.1021/acs.langmuir.0c00824
Langmuir 2020, 36, 6736−6748

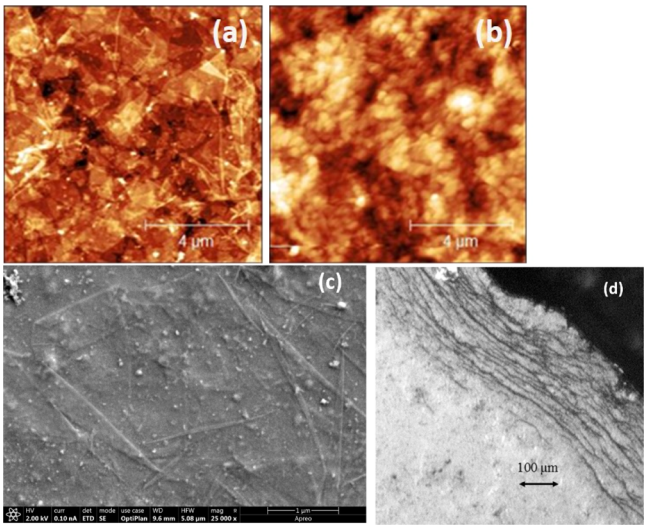

Figure 2. AFM images of spin-sprayed (a) $(PP/Ce/GO/Ce)_3$/PEDOT and (b) $(PP/Ce/GO/Ce)_{20}$/PEDOT films; (c) SEM image of a $(PP/Ce/GO/Ce)_{15}$ film (with 16 nm evaporated carbon surface film) and (d) light microscopy image of the edge of a $(PP/Ce/GO/Ce)_{100}$ film.

without GO.[4,7] At a larger scale, the films appear smooth and uniform (Figure S2). It may be noted that spinning is essential for the formation of smooth films because sprayed-only films contain aggregated GO sheets.[55] In contrast to the dipping method, spin and spin-spray coating tend to orient polyelectrolytes and the GO flakes on the surface.[72,73] The linear growth and leveling of the surface roughness imply a more or less stratified structure of the spin-sprayed $(PP/Ce/GO/Ce)_n$ multilayers, which is also supported by the light microscopy images of the terraced edges of the films (Figure 2).

Surface Polymerization of PEDOT. The polymerization of PEDOT onto the oxidative film from an adjacent pH 1.5 aqueous EDOT solution was followed by UV−vis spectroscopy. The use of low pH is advantageous because the oxidation potential of the Ce(III)/Ce(IV) redox pair increases with decreasing pH.[5,7] Transfer of the films from acidic solution to pure water causes small changes in their spectra, which are characteristic of the dedoping of the polymer (Figure S4).[74,75] The acidity of the solution has been shown to affect the apparent oxidation state of PEDOT films because of protonic doping,[76,77] but the nascent polymer film is in a highly oxidized state.

The polymerization of PEDOT on the oxidative films is a complicated process, but it can be divided into two main processes.[7] In the primary reaction, Ce(IV) oxidizes EDOT monomers to radical cations ($EDOT^{+\bullet}$) and is reduced to Ce(III). The initial amount of Ce(IV) in the oxidative film limits the oxidation process. The second process is the further reaction of the radical cations with EDOT monomers to form an oxidized polymer chain. These processes, cerium reduction and PEDOT formation, can be followed spectroscopically, and the absorbance changes of the spin-spray LbL $(PP/Ce/GO/Ce)_n$/PEDOT films during the polymerization are similar to those seen with dip LbL films (Figure S3).[4,5,7] The absorbance decreases at 300 nm as Ce(IV) is reduced to Ce(III) and increases above 400 nm because of the formation of an oxidized polymer film. A third, much slower process is observed during the final stages of polymerization, characterized by absorbance increase at *ca.* 800 nm and decrease above 900 nm. A similar slow process was also seen with dip LbL oxidative multilayers.[7] In polythiophenes, the charged quasiparticles in the polymer chains have been classified as polarons (one positive charge) and bipolarons (doubly charged), and the spectral features have been assigned to these species.[78] The semi-empirical models used allow us to accommodate two polarons in a single polymer chain, but recent theoretical calculations utilizing density functional theory (DFT) have offered a more multifaceted picture.[79,80] According to this model, the oxidation of the polymer chain introduces multiple charges in the chain, and systems with an odd or even number of positive charges represent polaronic or bipolaronic states, respectively. The states differ in their spin values, but most of them produce levels in the band gap and give rise to transitions in the visible and near-IR range. Accordingly, the final stages of the spectral behavior of the nascent PEDOT film can be assigned to slow charge redistribution within the polymer matrix, in which charge is diffusing and equalizing between the initially highly oxidized polymer segments around the cerium atoms and the polymer chains with a lower oxidation level.

The kinetics of the PEDOT polymerization process was evaluated at 310, 840, and 1000 nm, corresponding to the Ce(IV) reduction, PEDOT formation, and the charge redistribution processes, respectively (see the Supporting Information and Figure S5 for details). It should be noted that the two last reactions are complex processes involving various monomer and radical couplings and oxidation and disproportionation-like reactions of the polymer. However, they were all found to follow the first-order kinetics, and the corresponding pseudo-first-order rate constants k_{Ce}, k_{PEDOT}, and k_{disp} are shown in Figure 3 as a function of the oxidative

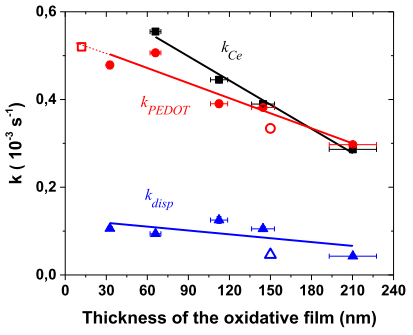

Figure 3. Rate constants for the reduction of Ce(IV) (k_{Ce}, black), for the formation of PEDOT (k_{PEDOT}, red), and for the slow equalization of the oxidation state of PEDOT by charge redistribution (k_{disp}, blue). The lines represent linear fits to the data. Open symbols show the k_{PEDOT} or k_{disp} values for dip LbL-fabricated $(PP/Ce)_5$ (red square) and $(PP/Ce/GO/Ce)_4$ (red circle and blue triangle) multilayers.[5,7]

multilayer thickness. The rate constants for the two main reactions, Ce reduction and PEDOT formation, decrease approximately linearly with thickness, which illustrates the heterogeneous nature of these reactions. Both processes continue simultaneously until all available oxidants are used. In thick multilayers, mass transfer of the reactants becomes more difficult and slows the film formation. Although the time constant of the PEDOT formation decreases from *ca.* 30 min with thin oxidative films to *ca.* 1 h with thick ones, the reaction is practically complete within a few hours even with thick films.

https://dx.doi.org/10.1021/acs.langmuir.0c00824
Langmuir 2020, 36, 6736−6748

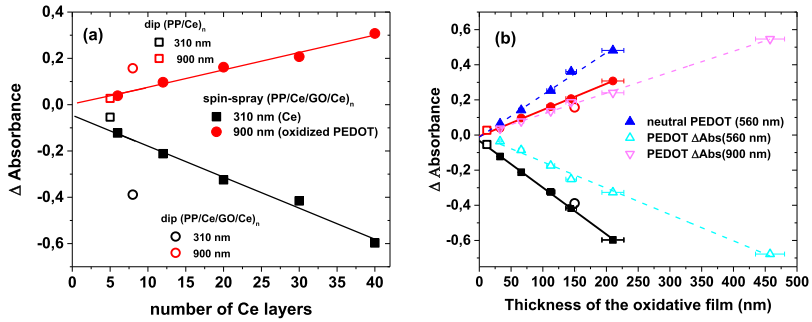

Figure 4. Absorbance change due to polymerization of PEDOT at 310 and 900 nm, corresponding to the loss of Ce(IV) and the formation of oxidized PEDOT, respectively, on spin-spray and dip LbL[5,7] $(PP/Ce/GO/Ce)_n$ or $(PP/Ce)_n$ multilayers. In (a), as a function of the number of Ce layers and in (b), as a function of the thickness of the oxidative film. (b) Absorbance of the completely reduced PEDOT (560 nm, absorbance of the (PP/Ce/rGO/Ce) multilayer subtracted) and the difference at 560 and 900 nm between completely oxidized (+0.8 V) and reduced (−1.1 V) PEDOT.

The apparent rate of charge redistribution is practically independent of thickness, which shows that it is a homogeneous process taking place within the formed PEDOT film. Results for two dip LbL oxidative films are also included in Figure 3,[5,7] and they show that neither the presence of GO nor the fabrication method has any significant effect on the polymerization rate or charge equilibration processes with films of similar thickness.

The absorbance changes at 310 and 900 nm during the film formation are proportional to the amounts of active oxidant and the as-formed PEDOT film, respectively (Figure 4), and they depend linearly on the thickness of the oxidative multilayer. Based on the absorbance changes, the oxidation capacity of the spin-spray LbL (PP/Ce/GO/Ce) multilayers is higher than that of the dip LbL (PP/Ce) multilayers but lower than with dip LbL (PP/Ce/GO/Ce) multilayers with the same amount of Ce layers (Figure 4a). Therefore, incorporation of GO into the oxidative multilayers increases the amount of bound oxidant per nominal Ce layer, more with dip LbL films. However, the number of oxidative tetralayers is not a reasonable parameter when discussing the oxidative capacity of the films. More valuable information is obtained by looking at the oxidative film thickness, and, in terms of it, the amounts of both the reactive oxidant and the as-deposited polymer seem to be practically independent of the method of multilayer preparation (Figure 4b). With spin-sprayed multilayers, the active oxidant content and the amount of formed polymer increase linearly with the thickness of the oxidative film. Although it is possible to produce thick GO-containing films with few layers by the dip LbL technique, the spin-spray method is much faster, leads to more organized and smoother films, and can be easily extended to still thicker films.

Electrochemistry of the Polymer Films. The as-made $(PP/Ce/GO/Ce)_n$/PEDOT films exhibit two different electrochemical processes, the irreversible reduction of GO to reduced GO and the reversible oxidation−reduction of PEDOT. These redox processes are independent of each other, and PEDOT redox cycling can be carried out prior to or after the GO reduction. However, the reduction of GO takes place already below −0.4 V *versus* Ag/AgCl,[81,82] at which potential PEDOT is not yet completely reduced and is practically completed within a single voltammetric sweep, irrespective of the film thickness (Figure S7). The reduction slightly increases the film absorption over a wide range (Figure S6), probably because of increased scattering, but has no effect on the spectral behavior of PEDOT (Figure S6). *In situ* UV−vis difference spectra for the reduction (from −0.1 to −1.1 V) and oxidation (from +0 to +0.8 V) of the $(PP/Ce/rGO/Ce)_{40}$/PEDOT film are shown in Figure S9, and typical absorbance changes for the PEDOT-based material are seen in the spectra.

In addition to the two redox processes discussed above, the films contain redox-active cerium also. However, the redox pair Ce(IV)/Ce(III) is generally very sluggish and was not observed in the (PP/Ce) multilayers without a polypyrrole coating.[4,5] A cerium-based slow redox reaction is also seen in (PP/Ce/rGO/Ce) multilayers before the deposition of a PEDOT film but not after it (Figures S8 and S10). Therefore, Ce(IV)/Ce(III) electroactivity, within the time scale of the experiments, requires the presence of a conductive material capable of coordinating to the metal, either pyrrole or rGO.[7] Thiophene moieties, on the other hand, are poorly coordinating, and PEDOT cannot act as an electron mediator to the metal redox pair. It also prevents its electrical interaction with rGO, possibly by effectively encapsulating the cerium ions during the polymerization process.

The relative amount of electroactive PEDOT as a function the film thickness was determined by UV−vis spectroelectrochemistry. Graphene oxide was reduced to rGO before the measurements because the complete reduction of PEDOT requires more cathodic potentials than the GO reduction. The absorbance of the totally reduced PEDOT film at the maximum wavelength of the $\pi \rightarrow \pi^*$ transition (*ca.* 560 nm, the absorbance of the (PP/Ce/rGO/Ce) multilayer subtracted, see the Supporting Information), in Figure 4, shows that the amount of redox-active polymer depends linearly on the thickness of the oxidative multilayer. The same conclusion is obtained from the absorbance difference between the fully reduced and oxidized polymers. The difference spectra of the oxidized and reduced films (measured at +0.8 and −1.1 V *vs* Ag/AgCl, respectively; no spectral changes were seen outside this potential range) were identical in shape with all multilayers studied (Figure S11), and the absorbance changes at 560 and 900 nm are shown in Figure 4 as a function of the thickness of the oxidative multilayer. Therefore, the amount of electroactive PEDOT is linearly dependent on the thickness of the underlying oxidative film. Because the total amount of PEDOT formed is also linearly dependent on the oxidative film thickness (Figures 1 and 4), this shows that the fraction of the electroactive polymer is independent of the film thickness. In addition, the spectra of reduced PEDOT (Figure S10) allow an independent estimation of the effective thickness of the

https://dx.doi.org/10.1021/acs.langmuir.0c00824
Langmuir 2020, 36, 6736−6748

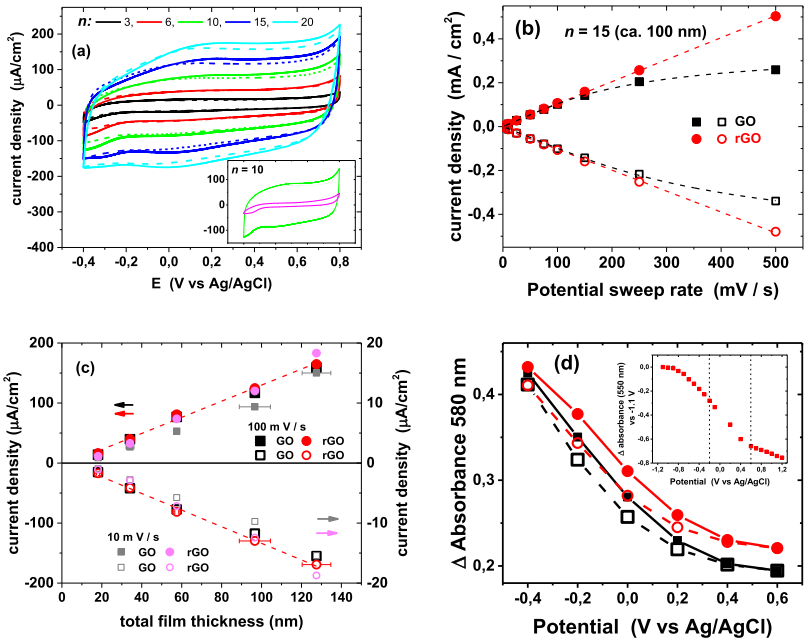

Figure 5. (a) Cyclic voltammograms of the $(PP/Ce/GO/Ce)_n$/PEDOT films before (dashed lines) and after (solid lines) the reduction of GO (sweep rate 100 mV/s). The inset shows cyclic voltammograms of the $(PP/Ce/GO/Ce)_{10}$/PEDOT film with 10 mV/s (magenta) and 100 mV/s (green) sweep rates. (b) Oxidation (positive) and reduction (negative) current in the voltammograms of a $(PP/Ce/GO/Ce)_{15}$/PEDOT film (at +0.1 V) as a function of the potential sweep rate. Dashed lines are linear (red) or RC-model (black) fits to data. (c) Effect of the total film thickness on current (at +0.1 V) before and after GO reduction to rGO. Dashed lines are linear fits to data after GO reduction, and standard deviation of thickness measurements is shown only for some symbols for clarity. Note that the scale on the left current axis is 10× that of the right axis. (d) Absorbance changes of a $(PP/Ce/GO/Ce)_{20}$/PEDOT film at 580 nm during oxidation (solid symbols and lines) and reduction (open symbols and dashed lines) before (black) and after (red) GO reduction to rGO. The inset shows the absorbance changes of a $(PP/Ce/rGO/Ce)_{40}$/PEDOT film (referenced to a neutral PEDOT film at −1.1 V) over a wider potential range. Dashed lines show the range used in the analysis.

polymer film formed using the reported complex dielectric function of neutral PEDOT (at 594 nm), and these thickness values are shown in Figure 1a (see the Supporting Information for details).[83]

Film Capacitance. Cyclic voltammetry is an excellent technique to obtain a general picture of any electrochemical processes. In addition to a qualitative understanding of the redox reactions involved, it allows a rapid screening of the capacitive behavior of the films. Graphene oxide sheets are insulating, and $(PP/Ce/GO/Ce)_n$/PEDOT films were studied electrochemically using cyclic voltammetry (from −0.4 to +0.8 V) both before and after the electrochemical reduction of GO in order to see whether it has any effect on the film properties. According to the spectroelectrochemical studies mentioned above, the oxidation state of Ce(III) remains unchanged in this potential range and no significant reduction of GO takes place. The anodic upper limit is set by the overoxidation of PEDOT. The cyclic voltammograms of the $(PP/Ce/GO/Ce)_n$/PEDOT films in this potential range are shown in Figure 5a (and in Figure S12). In the range from −0.4 to +0.8 V, the voltammograms are almost rectangular at high (100 mV/s) and low (10 mV/s) scan rates, which is typical for capacitive processes, and the current is linearly dependent on the film thickness with both scan rates (Figure 5c), especially after the reduction of GO. Similar linear dependence on PEDOT film thickness has been previously reported for the capacitive current, while the faradaic current of redox species in solution is only slightly affected.[84] This implies that the PEDOT film is porous enough to allow a free movement of the small electrolyte ions in solution but blocks larger species, which react mainly at the film/solution interface. In addition, the effect of the potential sweep rate was tested with a $(PP/Ce/GO/Ce)_{15}$/PEDOT film (thickness *ca.* 100 nm, Figure 1a), and the current is linearly dependent on the sweep rate after the reduction of GO (Figure 5b; note also the 10-fold difference in the scales of the two *y*-axis in Figure 5c; a linear dependence of current at +0.1 V on the scan rate was also observed with (PP/Ce/rGO/Ce) multilayers, see Figure S8), which shows that diffusion is not a limiting factor. Especially, GO sheets do not hamper the counterion diffusion. The linear dependence of current on thickness also shows that the fraction of electroactive PEDOT is thickness-independent on the voltammetric time scale, which is much smaller than that of the equilibrium spectroelectrochemical measurements, in Figure 4. The spectra display only a small effect of GO reduction on the observed redox changes in PEDOT (Figure 5d), and the positive shift in the absorbance can be attributed to increased scattering. However, there is a negative deviation from linearity (both with thickness and sweep rate) in current before the reduction of GO, and this effect can be described using a simple RC circuit model (dashed lines in Figure 5b; see the Supporting Information). The time constant of the film is high before GO reduction, and this can be attributed to a large charge transfer resistance across the film (*ca.* 1.4 kΩ cm^2 during oxidation for a $(PP/Ce/GO/Ce)_{15}$/PEDOT film; the effective resistance is lower during the reduction sweep because the film is in a conducting state). The GO sheets slow down the charge transfer kinetics in the films because of their insulating nature but do not deactivate the polymer.

The film capacitance was estimated from the third voltammetric cycles in the intermediate potential range (from −0.2 to +0.6 V *vs* Ag/AgCl), according to eq 1,

https://dx.doi.org/10.1021/acs.langmuir.0c00824
Langmuir 2020, 36, 6736−6748

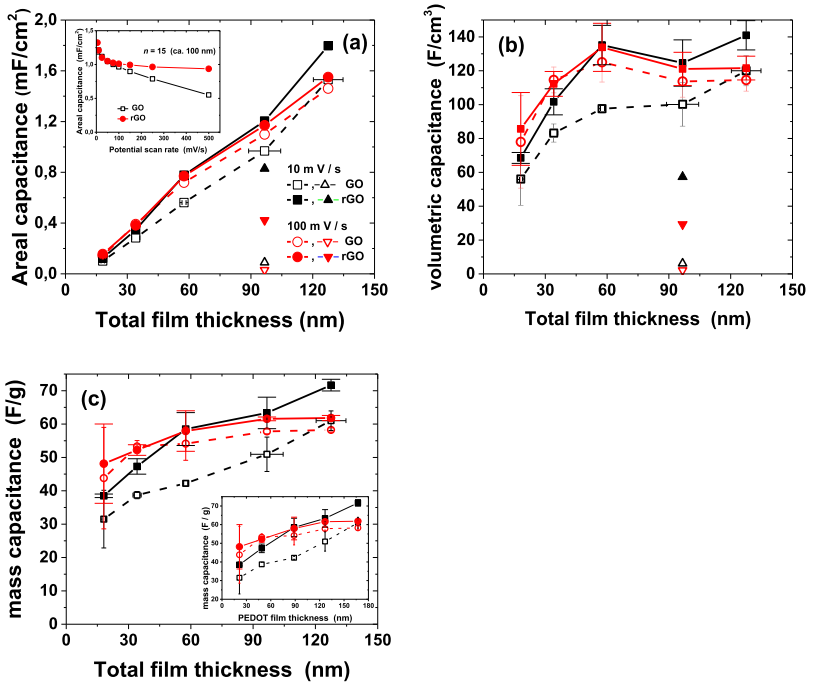

Figure 6. Specific (a) areal (mF/cm^2), (b) volumetric (F/cm^3), and (c) mass capacitance (per mass of PEDOT, F/g) of the $(PP/Ce/GO/Ce)_n$/PEDOT films measured in a three-electrode configuration with 10 mV/s (black symbols and lines) and 100 mV/s (red) sweep rates before and after the reduction of GO to rGO (open and solid squares or circles, respectively). The capacitance of the $(PP/Ce/GO/Ce)_{15}$ multilayer without PEDOT shown in (a,b) before and after GO reduction (open and solid triangles, respectively) at the total thickness corresponding to a PEDOT-covered multilayer. The inset in (c) shows the mass specific capacitance as a function of PEDOT film thickness. Lines are just a guide to the eye, and standard deviation of thickness measurements is shown only for one curve for clarity. Capacitance error bars for films with rGO enhanced using wider end gaps.

where v is the sweep rate and $E_{1,2}$ denote the end point potentials. This limited potential range does not utilize the whole available electrochemical window of PEDOT, but it was used in order to compare the effect of GO reduction on the capacitance values.

$$C = \frac{1}{2v|E_2 - E_1|}\int_{E_1}^{E_2} |I| dE \quad (1)$$

The dependence of the specific capacitance of the films with respect to their geometrical area and volume, calculated using the macroscopic area of the film and the total film thickness (Figure 1), is shown in Figure 6a,b as a function of the total film thickness. The areal capacitance exhibits a nearly linear dependence on the film thickness, both before and after the reduction of GO in the film, and GO reduction leads only to a small increase. The potential scan rate has a negligible effect, especially after GO reduction. On the other hand, the volumetric capacitance seems to level off after *ca.* 60 nm, which corresponds to an approximate oxidative film thickness of 110 nm (10 (PP/Ce/GO/Ce) tetralayers) and the leveling of the surface roughness (Figure 1). The maximum volumetric capacitance obtained for a $(PP/Ce/(r)GO/Ce)_n$/PEDOT film is 120−140 F cm^{-3}. An independent estimation for the specific capacitance per mass of PEDOT (note that this is not per mass of the total film) can be obtained from the optically determined thickness of the PEDOT film (Figure 1) and the areal capacitance, using 1.5 g cm^{-3} as the density of neutral PEDOT.[83,85,86] Because the PEDOT film thickness depends linearly on the number of tetralayers in the oxidative multilayer, the behavior of the specific mass capacitance closely mirrors that of the volumetric capacitance and reaches values of 60−70 F g^{-1} with thicker films. Preliminary electrochemical stability measurements showed that at least 90% of the initial capacitance is retained after 500 cycles, similar to that of a multilayer of PEDOT and graphene.[87]

The contribution of GO on the film capacitance was also studied using a film with 15 oxidative tetralayers without PEDOT (Figure 6a,b). Before GO reduction, the capacitance of the bare multilayer is negligible but amounts up to two-thirds of the areal capacitance of a similar film with PEDOT after the reduction, under the same experimental conditions. The volume capacitance (calculated per volume of the film before PEDOT deposition) displays similar behavior but the values are lower, maximally 50% of the capacitance in the presence of PEDOT. However, the capacitance without PEDOT is highly dependent on the potential sweep rate, which shows that the charge transfer in the $(PP/Ce/rGO/Ce)_n$ films is slow because of the low conductivity of the rGO or insufficient percolation. In the PEDOT-containing film, the oxidation state of GO has only a small effect on capacitance, although its effect on charge transfer rate is more pronounced (Figure 5). Therefore, PEDOT is required in the film to impose electrical connection throughout the film and to obtain a highly redox-active film with fast charge transfer kinetics. Interestingly, the contributions from rGO and PEDOT do not seem to be additive, and part of the rGO/solution interfacial capacitance is lost when the sheets become wrapped with the polymer. As mentioned above, the Ce(IV/III) pair is also redox-active in the rGO-containing multilayers before, but not after, the PEDOT deposition. However, this pair is kinetically so sluggish that its contribution is negligible in the voltammetric time scale.

https://dx.doi.org/10.1021/acs.langmuir.0c00824
Langmuir 2020, 36, 6736−6748

The reported capacitance values in the literature cover a wide range because of different preparation methods, composition, and measurement conditions. In addition, with thin films, the measurement of the film thickness or mass is prone to errors. Typical values for the specific volumetric capacitance for PEDOT-based materials range from *ca.* 30 F cm^{-3} to *ca.* 330 F cm^{-3}.[14,17,88] Based on electrochemical considerations or DFT calculations, the theoretical specific capacitance of pure PEDOT has been estimated to be *ca.* 210 F g^{-1} or 100 F cm^{-3}.[24,85] Nanostructured PEDOT-based films were reported to have a specific mass capacitance in the range 110−150 F g^{-1}.[89] PEDOT is often applied as a polyelectrolyte complex with PSS, and a recent study attributes the pseudocapacitive behavior of PEDOT-PSS electrodes to the double-layer charging at the domain boundaries between PEDOT-rich and PSS-rich microphases, giving rise to a volumetric capacitance of 34 F cm^{-3}.[17] A similar value of 39 F cm^{-3} has been obtained using electrochemical transistors.[14]

The error estimates for the capacitance values are relatively large, especially with thinner films, and these errors originate mainly from the uncertainty in the total film thickness. On the other hand, the effective thickness of the PEDOT layer is obtained using spectroscopic data, and these values are more precise (there might be systematic errors because of uncertainty in the optical parameters). Therefore, the specific mass capacitance, calculated per mass of PEDOT, displays smaller errors and behaves more smoothly as a function of total film or PEDOT layer thickness. The behavior of capacitance as a function of film thickness is interesting because there are only very few papers dealing with the thickness dependence. The capacitive current has been shown to increase linearly with film thickness, as was also observed in this work (Figure 5c), which implies linear dependence of the areal capacitance on thickness and a constant volumetric capacitance.[84] With much thicker PEDOT/poly(ethylene oxide) networks, the specific mass capacitance was constant until finally decreasing when ion diffusion becomes a limiting factor (above *ca.* 100 μm).[90] A roughly linear relation between the observed capacitance and film thickness was also observed with PEDOT/PSS transistors below 1 μm.[14] A constant mass specific capacitance (92 F g^{-1}) was obtained for electropolymerized PEDOT films.[91] Therefore, the values obtained in this work are well in accordance with the published specific capacitances. A change in observed volumetric or mass capacitance would imply changes in film structure with thickness. Although it would be tempting to assume that the observed capacitance of thin films displays thickness-dependent contributions from, for example, interfacial and bulk (redox) capacitance, we attribute the apparent change to experimental errors and, especially, to the non-zero intercepts of the areal capacitance *versus* thickness plots (Figures 6a and S14). Very thin films do not form a homogeneous cover on the surface, and the observed behavior will deviate from ideal.

The microscopic nature of the capacitance on PEDOT-based electrodes has been considered recently. Mathematical models based on coupled ion−electron diffusion and migration have been shown to reproduce the form of the cyclic voltammogram without any assumption of faradaic processes.[17] DFT calculations suggest charge storage in nanocapacitors formed between the polymer chain and the counterion.[85] We have measured the spectral behavior of the films over a wide potential range (Figure 5d) in the spectral range of the $\pi \rightarrow \pi^*$(HOMO−LUMO) transition in PEDOT, which is less affected by the complicated spectral features of the polaronic and bipolaronic states than spectral behavior above 700 nm. Clear spectral changes take place within the potential range used for the capacitance determination, showing that PEDOT reduction and oxidation take place within the whole potential window. The effect of GO reduction is very small, and the PEDOT/rGO (or GO) interfaces do not significantly contribute to the overall capacitance (Figure 6). In fact, the polymer reduces the contribution from the rGO/solution interface. Therefore, even with the thin films containing PEDOT, we attribute the observed capacitance mainly to the doping−dedoping process of PEDOT, which charges and discharges the polaron/bipolaron—counterion nanocapacitors.[85]

All the films studied here are rather thin, below 200 nm, and at the moment, we have not enough data to reliably extrapolate the properties to much thicker films. However, after the reduction of GO, the behavior of the current with the film thickness suggests that charge transfer kinetics is unlikely to become an important limiting factor in thicker films. A thorough assessment of the application potentials of the films as capacitive elements will, however, require more detailed studies of the charge transfer kinetics, as well as measurements using the two-electrode configuration, and these will be covered in our ongoing work. In addition to the (PP/Ce/GO/Ce)/PEDOT films, electroactive spin-spray LbL (PP/Ce/GO/Ce)/polydopamine films have been prepared in our laboratory from 5,6-dihydroxyindole.[6] Preliminary experiments show that the areal capacitance of a bioinspired $(PP/Ce/GO/Ce)_{20}$/polydopamine film at pH 7 (in a 0.1 M phosphate buffer containing 0.1 M KCl) is *ca.* 3.5 mF/cm^2 after the reduction of GO, even higher than that of the corresponding PEDOT-based film. The reduction of GO increased the capacitance of the polydopamine film by an order of magnitude, and the results highlight the potential of oxidative (PP/Ce/GO/Ce) multilayers as general platforms for capacitive films.

CONCLUSIONS

Coordinative (PP/Ce/GO/Ce) films are examples of reactive LbL multilayers and represent a general technology platform for the oxidative polymerization of conducting polymers into their structure. The addition of GO into the oxidative films increases the amount of cerium in the films per nominal Ce layer. Compared to the dip LbL technique, the spin-spray LbL film assembly is a much faster method for growing oxidative multilayers with repeating (PP/Ce/GO/Ce) tetralayer strata. The films grow linearly, and their surface roughness stays low (below 15 nm), contrary to the corresponding films prepared by the dip LbL technique, which display exponential growth and high roughness.

EDOT polymerizes on the $(PP/Ce/GO/Ce)_n$ multilayers and the amount of Ce(IV) in the oxidative film is the limiting factor in the polymerization process. The reduction of Ce(IV) and the formation of oxidized PEDOT follow the pseudo-first-order kinetics. After drying, the resulting $(PP/Ce/GO/Ce)_n$/PEDOT films are thinner than the oxidative films before polymerization. The initial amount of oxidant, Ce(IV), and the amount of polymerized PEDOT depend linearly on the thickness of the oxidative film. The effective thickness of the formed PEDOT film and the amount of redox-active polymer also increase linearly with the thickness of the oxidative multilayer.

https://dx.doi.org/10.1021/acs.langmuir.0c00824
Langmuir 2020, 36, 6736−6748

The electrochemical behavior of the PEDOT-covered films was studied before and after the reduction of GO to rGO. The PEDOT effectively fills the underlying oxidative film, which allows high electroactivity and facile charge transport without diffusion limitation in a voltammetric time scale. The current and redox changes also scale linearly with film thickness after the reduction of GO to rGO. The effect of the GO reduction can be attributed to a better conductivity of films containing rGO.

The work aims at facile preparation of biodegradable supercapacitors, and the $(PP/Ce/GO/Ce)_n$/PEDOT films were used as simple models. The capacitance values of the electrodes were determined by cyclic voltammetry. The specific areal capacitance scales linearly with the film thickness, reaching *ca.* 1.6 mF cm^{-2} with a $(PP/Ce/GO/Ce)_{20}$/PEDOT film. The specific volumetric (per volume of the whole film) and mass (per mass of PEDOT) capacitances were *ca.* 120−140 F cm^{-3} and 60−70 F g^{-1}, respectively, in accordance with literature values for pure PEDOT-based films. With films containing PEDOT, the GO or rGO sheets do not have a significant contribution to the capacitance at scan rates of 100 mV/s and below. Preliminary tests showed that at least 90% of the initial capacitance is retained after 500 potential cycles. In addition, preliminary experiments with polydopamine, a bioinspired redox-active material, yielded a capacitance of 3.5 mF/cm^2. Further studies on the stability of the films, their behavior in two-electrode configuration, and the charge transport kinetics and interfacial processes are in progress.

We have previously presented studies of oxidative multilayers based on dip LbL (PP/Ce) and (PP/Ce/GO/Ce) multilayers. The spin-spray technique allows a significantly faster deposition of multilayers. The incorporation of GO sheets into the structure always increases the surface roughness, significantly with the dip LbL technique, but results in films with higher oxidation capacity (more incorporated oxidant) per nominal Ce layer. However, even if the amount of deposited material per nominal layer or the kinetics of EDOT polymerization vary in differently prepared films, the effect of the film composition or fabrication technique is very small when comparing films of the same thickness. Therefore, the major and somewhat unexpected result of the work is that the reaction kinetics and the reactant capacity, important for these chemically reactive and redox-active multilayers, are not noticeably affected by the assembly technique. The GO sheets do not markedly influence the film capacity or charge transfer kinetics, and (especially after reduction) their main role in the PEDOT-containing films is in structural reinforcement and layer thickness enhancement. The deposited PEDOT affects the rGO/ambient interface in a subtle way which hampers the utilization of the benefits of the components in full. However, the results suggest that the spin-spray-assembled oxidative multilayers are promising platforms for the fabrication of capacitive films for charge storage applications, based on various polymerizable materials.

■ ASSOCIATED CONTENT

Supporting Information

The Supporting Information is available free of charge at https://pubs.acs.org/doi/10.1021/acs.langmuir.0c00824.

AFM and SEM images of the $(PP/Ce/GO/Ce)_n$ and $(PP/Ce/GO/Ce)_n$/PEDOT films, UV−vis spectra and kinetic fits of the polymerization of EDOT, electrochemical reduction of GO by cyclic voltammetry and its effect on the UV−vis spectra, electroactivity of bare oxidative films, *in situ* UV−vis spectra of the $(PP/Ce/rGO/Ce)_n$/PEDOT films, description of the method for the estimation of the amount of electroactive PEDOT and the effective thickness of the PEDOT layer, cyclic voltammograms and the specific areal and volumetric capacitance of the $(PP/Ce/GO/Ce)_n$/PEDOT films, RC circuit model and fits to the effect of sweep rate on current, and description of the method for the error estimation for the specific capacitance (PDF)

■ AUTHOR INFORMATION

Corresponding Authors

Mikko Salomäki − *Department of Chemistry, University of Turku, FI-20014 Turku, Finland; Turku University Centre for Surfaces and Materials (MatSurf), FI-20014 Turku, Finland;* orcid.org/0000-0001-6190-2073; Email: mikko.salomaki@utu.fi

Jukka Lukkari − *Department of Chemistry, University of Turku, FI-20014 Turku, Finland; Turku University Centre for Surfaces and Materials (MatSurf), FI-20014 Turku, Finland;* orcid.org/0000-0002-9409-7995; Email: jukka.lukkari@utu.fi

Authors

Lauri Marttila − *Department of Chemistry and Doctoral Programme in Physical and Chemical Sciences, University of Turku, FI-20014 Turku, Finland;* orcid.org/0000-0002-8221-0954

Henri Kivelä − *Department of Chemistry, University of Turku, FI-20014 Turku, Finland; Turku University Centre for Surfaces and Materials (MatSurf), FI-20014 Turku, Finland;* orcid.org/0000-0003-1414-8893

Matti Tupala − *Department of Chemistry, University of Turku, FI-20014 Turku, Finland*

Complete contact information is available at: https://pubs.acs.org/10.1021/acs.langmuir.0c00824

Author Contributions

L.M. carried out most of the experimental work, M.T. participated in the experimental work, M.S. and J.L. supervised the work, and L.M., J.L., M.S., and H.K. analyzed the results and wrote the article together.

Funding

L.M. gratefully acknowledges the Emil Aaltonen Foundation for a research grant (grant numbers 160165 N, 170166 N, and 180162 N).

Notes

The authors declare no competing financial interest.

■ ACKNOWLEDGMENTS

We are grateful to Dr Lippo Lassila, Turku Centre for Biomaterials, for the light microscopy images.

■ REFERENCES

(1) *Multilayer Thin Films: Sequential Assembly of Nanocomposite Materials*, 2nd ed.; Decher, G., Schlenoff, J. B., Eds.; Wiley-VCH Verlag GmbH & Co. KGaA: Weinheim, Germany, 2012.

(2) Fulghum, T. M.; Patton, D. L.; Advincula, R. C. Fuzzy Ternary Particle Systems by Surface-Initiated Atom Transfer Radical Polymer-

ization from Layer-by-Layer Colloidal Core−Shell Macroinitiator Particles. *Langmuir* **2006**, *22*, 8397−8402.
(3) Edmondson, S.; Vo, C.-D.; Armes, S. P.; Unali, G.-F.; Weir, M. P. Layer-by-Layer Deposition of Polyelectrolyte Macroinitiators for Enhanced Initiator Density in Surface-Initiated ATRP. *Langmuir* **2008**, *24*, 7208−7215.
(4) Salomäki, M.; Räsänen, M.; Leiro, J.; Huti, T.; Tenho, M.; Lukkari, J.; Kankare, J. Oxidative Inorganic Multilayers for Polypyrrole Film Generation. *Adv. Funct. Mater.* **2010**, *20*, 2140−2147.
(5) Salomäki, M.; Myllymäki, O.; Hätönen, M.; Savolainen, J.; Lukkari, J. Layer-by-Layer Assembled Oxidative Films as General Platform for Electrodeless Formation of Conducting Polymers. *ACS Appl. Mater. Interfaces* **2014**, *6*, 2325−2334.
(6) Salomäki, M.; Tupala, M.; Parviainen, T.; Leiro, J.; Karonen, M.; Lukkari, J. Preparation of Thin Melanin-Type Films by Surface-Controlled Oxidation. *Langmuir* **2016**, *32*, 4103−4112.
(7) Salomäki, M.; Kauppila, J.; Kankare, J.; Lukkari, J. Oxidative Layer-By-Layer Multilayers Based on Metal Coordination: Influence of Intervening Graphene Oxide Layers. *Langmuir* **2018**, *34*, 13171−13182.
(8) Shao, Y.; El-Kady, M. F.; Sun, J.; Li, Y.; Zhang, Q.; Zhu, M.; Wang, H.; Dunn, B.; Kaner, R. B. Design and Mechanisms of Asymmetric Supercapacitors. *Chem. Rev.* **2018**, *118*, 9233−9280.
(9) Najib, S.; Erdem, E. Current Progress Achieved in Novel Materials for Supercapacitor Electrodes: Mini Review. *Nanoscale Adv.* **2019**, *1*, 2817−2827.
(10) Meng, Q.; Cai, K.; Chen, Y.; Chen, L. Research Progress on Conducting Polymer Based Supercapacitor Electrode Materials. *Nano Energy* **2017**, *36*, 268−285.
(11) Kulandaivalu, S.; Sulaiman, Y. Recent Advances in Layer-by-Layer Assembled Conducting Polymer Based Composites for Supercapacitors. *Energies* **2019**, *12*, 2107.
(12) Zhao, Z.; Richardson, G. F.; Meng, Q.; Zhu, S.; Kuan, H.-C.; Ma, J. PEDOT-Based Composites as Electrode Materials for Supercapacitors. *Nanotechnology* **2015**, *27*, 042001.
(13) Lehtimäki, S.; Suominen, M.; Damlin, P.; Tuukkanen, S.; Kvarnström, C.; Lupo, D. Preparation of Supercapacitors on Flexible Substrates with Electrodeposited PEDOT/Graphene Composites. *ACS Appl. Mater. Interfaces* **2015**, *7*, 22137−22147.
(14) Rivnay, J.; Leleux, P.; Ferro, M.; Sessolo, M.; Williamson, A.; Koutsouras, D. A.; Khodagholy, D.; Ramuz, M.; Strakosas, X.; Owens, R. M.; Benar, C.; Badier, J.-M.; Bernard, C.; Malliaras, G. G. High-Performance Transistors for Bioelectronics through Tuning of Channel Thickness. *Sci. Adv.* **2015**, *1*, No. e1400251.
(15) Zhao, Q.; Wang, G.; Yan, K.; Yan, J.; Wang, J. Binder-Free Porous PEDOT Electrodes for Flexible Supercapacitors. *J. Appl. Polym. Sci.* **2015**, *1324142549*.
(16) Kurra, N.; Wang, R.; Alshareef, H. N. All Conducting Polymer Electrodes for Asymmetric Solid-State Supercapacitors. *J. Mater. Chem. A* **2015**, *3*, 7368−7374.
(17) Volkov, A. V.; Wijeratne, K.; Mitraka, E.; Ail, U.; Zhao, D.; Tybrandt, K.; Andreasen, J. W.; Berggren, M.; Crispin, X.; Zozoulenko, I. V. Understanding the Capacitance of PEDOT:PSS. *Adv. Funct. Mater.* **2017**, *27*, 1700329.
(18) Cheng, T.; Zhang, Y.-Z.; Zhang, J.-D.; Lai, W.-Y.; Huang, W. High-Performance Free-Standing PEDOT:PSS Electrodes for Flexible and Transparent All-Solid-State Supercapacitors. *J. Mater. Chem. A* **2016**, *4*, 10493−10499.
(19) Malti, A.; Edberg, J.; Granberg, H.; Khan, Z. U.; Andreasen, J. W.; Liu, X.; Zhao, D.; Zhang, H.; Yao, Y.; Brill, J. W.; Engquist, I.; Fahlman, M.; Wågberg, L.; Crispin, X.; Berggren, M. An Organic Mixed Ion−Electron Conductor for Power Electronics. *Adv. Sci.* **2016**, *3*, 1500305.
(20) D'Arcy, J. M.; El-Kady, M. F.; Khine, P. P.; Zhang, L.; Lee, S. H.; Davis, N. R.; Liu, D. S.; Yeung, M. T.; Kim, S. Y.; Turner, C. L.; Lech, A. T.; Hammond, P. T.; Kaner, R. B. Vapor-Phase Polymerization of Nanofibrillar Poly(3,4-Ethylenedioxythiophene) for Supercapacitors. *ACS Nano* **2014**, *8*, 1500−1510.
(21) Han, Y.; Shen, M.; Wu, Y.; Zhu, J.; Ding, B.; Tong, H.; Zhang, X. Preparation and Electrochemical Performances of PEDOT/Sulfonic Acid-Functionalized Graphene Composite Hydrogel. *Synth. Met.* **2013**, *172*, 21−27.
(22) Karlsson, C.; Nicholas, J.; Evans, D.; Forsyth, M.; Strømme, M.; Sjödin, M.; Howlett, P. C.; Pozo-Gonzalo, C. Stable Deep Doping of Vapor-Phase Polymerized Poly(3,4-Ethylenedioxythiophene)/Ionic Liquid Supercapacitors. *ChemSusChem* **2016**, *9*, 2112−2121.
(23) Zeng, B.; Chen, Y.; Bai, J. Facile Synthesis of Molybdenum Disulfide/Poly (3,4-Ethylenedioxythiophene) Composite Electrodes for High-Performance Flexible Supercapacitors. *J. Mater. Sci.: Mater. Electron.* **2019**, *30*, 17706−17714.
(24) Lota, K.; Khomenko, V.; Frackowiak, E. Capacitance Properties of Poly(3,4-Ethylenedioxythiophene)/Carbon Nanotubes Composites. *J. Phys. Chem. Solids* **2004**, *65*, 295−301.
(25) Alvi, F.; Ram, M. K.; Basnayaka, P. A.; Stefanakos, E.; Goswami, Y.; Kumar, A. Graphene−Polyethylenedioxythiophene Conducting Polymer Nanocomposite Based Supercapacitor. *Electrochim. Acta* **2011**, *56*, 9406−9412.
(26) Chu, C.-Y.; Tsai, J.-T.; Sun, C.-L. Synthesis of PEDOT-Modified Graphene Composite Materials as Flexible Electrodes for Energy Storage and Conversion Applications. *Int. J. Hydrogen Energy* **2012**, *37*, 13880−13886.
(27) Zhou, H.; Yao, W.; Li, G.; Wang, J.; Lu, Y. Graphene/Poly(3,4-Ethylenedioxythiophene) Hydrogel with Excellent Mechanical Performance and High Conductivity. *Carbon* **2013**, *59*, 495−502.
(28) Sun, D.; Jin, L.; Chen, Y.; Zhang, J.-R.; Zhu, J.-J. Microwave-Assisted In Situ Synthesis of Graphene/PEDOT Hybrid and Its Application in Supercapacitors. *Chempluschem* **2013**, *78*, 227−234.
(29) Zhang, J.; Zhao, X. S. Conducting Polymers Directly Coated on Reduced Graphene Oxide Sheets as High-Performance Supercapacitor Electrodes. *J. Phys. Chem. C* **2012**, *116*, 5420−5426.
(30) Wen, J.; Jiang, Y.; Yang, Y.; Li, S. Conducting Polymer and Reduced Graphene Oxide Langmuir−Blodgett Films: A Hybrid Nanostructure for High Performance Electrode Applications. *J. Mater. Sci.: Mater. Electron.* **2014**, *25*, 1063−1071.
(31) Yang, Y.; Zhang, L.; Li, S.; Yang, W.; Xu, J.; Jiang, Y.; Wen, J. Electrochemical Performance of Conducting Polymer and Its Nanocomposites Prepared by Chemical Vapor Phase Polymerization Method. *J. Mater. Sci.: Mater. Electron.* **2013**, *24*, 2245−2253.
(32) Ates, M.; Bayrak, Y.; Ozkan, H.; Yoruk, O.; Yildirim, M.; Kuzgun, O. Synthesis of RGO/TiO2/PEDOT Nanocomposites, Supercapacitor Device Performances and Equivalent Electrical Circuit Models. *J. Polym. Res.* **2019**, *26*, 49.
(33) Ates, M.; Serin, M. A.; Calisskan, S. Electrochemical Supercapacitors of PANI/MWCNT, PEDOT/MWCNT and P-(ANI-Co-EDOT)/MWCNT Nanocomposites. *Polym. Bull.* **2019**, *76*, 3207−3231.
(34) Zhang, W.; Hou, L.; Zhou, H. Electrochemically Treated Graphite/Poly(3,4-Ethylenedioxythiophene)-Carbon Nanotubes Electrode: Facile Preparation and Remarkable Enhancement in Electrochemical Performances. *Fullerenes, Nanotubes, Carbon Nanostruct.* **2020**, *28*, 458.
(35) Ranjusha, R.; Sajesh, K. M.; Roshny, S.; Lakshmi, V.; Anjali, P.; Sonia, T. S.; Sreekumaran Nair, A.; Subramanian, K. R. V.; Nair, S. V.; Chennazhi, K. P.; Balakrishnan, A. Supercapacitors Based on Freeze Dried MnO2 Embedded PEDOT: PSS Hybrid Sponges. *Microporous Mesoporous Mater.* **2014**, *186*, 30−36.
(36) Hou, Y.; Cheng, Y.; Hobson, T.; Liu, J. Design and Synthesis of Hierarchical MnO2 Nanospheres/Carbon Nanotubes/Conducting Polymer Ternary Composite for High Performance Electrochemical Electrodes. *Nano Lett.* **2010**, *10*, 2727−2733.
(37) Zhuzhelskii, D. V.; Tolstopjatova, E. G.; Eliseeva, S. N.; Ivanov, A. V.; Miao, S.; Kondratiev, V. V. Electrochemical Properties of PEDOT/WO3 Composite Films for High Performance Supercapacitor Application. *Electrochim. Acta* **2019**, *299*, 182−190.
(38) Guan, X.; Zhao, L.; Zhang, P.; Song, X.; Liu, J.; Gao, L. Self-Supporting Electrode of High Conductive PEDOT:PSS/CNTs

https://dx.doi.org/10.1021/acs.langmuir.0c00824
Langmuir 2020, 36, 6736−6748

Coaxial Nanocables Wrapped by MnO2 Nanosheets. *ChemistrySelect* **2019**, *4*, 2009−2017.
(39) Salomäki, M.; Peltonen, T.; Kankare, J. Multilayer Films by Spraying on Spinning Surface — Best of Both Worlds. *Thin Solid Films* **2012**, *520*, 5550−5556.
(40) Salomäki, M.; Jaakkola, O.; Hirvonen, S.-P.; Tenhu, H.; Kvarnström, C. Highly Controllable Ambient Atmosphere Spray Deposition of Water Dispersible Poly-(Benzimidazobenzophenanthroline) Films. *Synth. Met.* **2018**, *245*, 144−150.
(41) Richardson, J. J.; Björnmalm, M.; Caruso, F. Technology-Driven Layer-by-Layer Assembly of Nanofilms. *Science* **2015**, *348*, aaa2491.
(42) Merrill, M. H.; Sun, C. T. Fast, Simple and Efficient Assembly of Nanolayered Materials and Devices. *Nanotechnology* **2009**, *20*, 075606.
(43) Schlenoff, J. B.; Dubas, S. T.; Farhat, T. Sprayed Polyelectrolyte Multilayers. *Langmuir* **2000**, *16*, 9968−9969.
(44) Schaaf, P.; Voegel, J.-C.; Jierry, L.; Boulmedais, F. Spray-Assisted Polyelectrolyte Multilayer Buildup: From Step-by-Step to Single-Step Polyelectrolyte Film Constructions. *Adv. Mater.* **2012**, *24*, 1001−1016.
(45) Dierendonck, M.; De Koker, S.; De Rycke, R.; De Geest, B. G. Just Spray It − LbL Assembly Enters a New Age. *Soft Matter* **2014**, *10*, 804−807.
(46) Gittleson, F. S.; Kohn, D. J.; Li, X.; Taylor, A. D. Improving the Assembly Speed, Quality, and Tunability of Thin Conductive Multilayers. *ACS Nano* **2012**, *6*, 3703−3711.
(47) Larocca, N. M.; Filho, R. B.; Pessan, L. A. Influence of Layer-by-Layer Deposition Techniques and Incorporation of Layered Double Hydroxides (LDH) on the Morphology and Gas Barrier Properties of Polyelectrolytes Multilayer Thin Films. *Surf. Coat. Technol.* **2018**, *349*, 1−12.
(48) Gittleson, F. S.; Hwang, D.; Ryu, W.-H.; Hashmi, S. M.; Hwang, J.; Goh, T.; Taylor, A. D. Ultrathin Nanotube/Nanowire Electrodes by Spin−Spray Layer-by-Layer Assembly: A Concept for Transparent Energy Storage. *ACS Nano* **2015**, *9*, 10005−10017.
(49) Min, S. j.; Yun Lee, S.; Lee, J. Y.; Lee, S.; Ho Choi, K.; Shin, G. Layer Contribution Model for Layer-by-Layer Self-Assembly Oxygen Barrier Film. *Mol. Cryst. Liq. Cryst.* **2017**, *658*, 127−130.
(50) Yang, F.; Li, C.; Xu, W.; Cai, Z. Multifunctional Antifogging Coatings Based on ZrO 2 and SiO 2 Nanoparticles by Spray-Spin-Blow Layer-by-Layer Assembly. *J. Mater. Res.* **2019**, *34*, 3827−3836.
(51) Zhao, Y.; Zhang, Z.; Shi, L.; Zhang, F.; Li, S.; Zeng, R. Corrosion Resistance of a Self-Healing Multilayer Film Based on SiO2 and CeO2 Nanoparticles Layer-by-Layer Assembly on Mg Alloys. *Mater. Lett.* **2019**, *237*, 14−18.
(52) Weng, G.-M.; Li, J.; Alhabeb, M.; Karpovich, C.; Wang, H.; Lipton, J.; Maleski, K.; Kong, J.; Shaulsky, E.; Elimelech, M.; Gogotsi, Y.; Taylor, A. D. Layer-by-Layer Assembly of Cross-Functional Semi-Transparent MXene-Carbon Nanotubes Composite Films for Next-Generation Electromagnetic Interference Shielding. *Adv. Funct. Mater.* **2018**, *28*, 1803360.
(53) Izquierdo, A.; Ono, S. S.; Voegel, J.-C.; Schaaf, P.; Decher, G. Dipping versus Spraying: Exploring the Deposition Conditions for Speeding Up Layer-by-Layer Assembly. *Langmuir* **2005**, *21*, 7558−7567.
(54) Krogman, K. C.; Zacharia, N. S.; Schroeder, S.; Hammond, P. T. Automated Process for Improved Uniformity and Versatility of Layer-by-Layer Deposition. *Langmuir* **2007**, *23*, 3137−3141.
(55) Hong, J.; Kang, S. W. Carbon Decorative Coatings by Dip-, Spin-, and Spray-Assisted Layer-by-Layer Assembly Deposition. *J. Nanosci. Nanotechnol.* **2011**, *11*, 7771−7776.
(56) Hong, J.; Park, H. Fabrication and Characterization of Block Copolymer Micelle Multilayer Films Prepared Using Dip-, Spin- and Spray-Assisted Layer-by-Layer Assembly Deposition. *Colloids Surf., A* **2011**, *381*, 7−12.
(57) Lee, T.; Yun, T.; Park, B.; Sharma, B.; Song, H.-K.; Kim, B.-S. Hybrid Multilayer Thin Film Supercapacitor of Graphene Nanosheets with Polyaniline: Importance of Establishing Intimate Electronic Contact through Nanoscale Blending. *J. Mater. Chem.* **2012**, *22*, 21092−21099.
(58) Sarker, A. K.; Hong, J.-D. Flexible and Transparent Plastic Electrodes Composed of Reduced Graphene Oxide/Polyaniline Films for Supercapacitor Application. *Bull. Korean Chem. Soc.* **2014**, *35*, 1799−1805.
(59) Tayel, M. B.; Soliman, M. M.; Ebrahim, S.; Harb, M. E. Sprayed Polyaniline Layer onto Chemically Reduced Graphene Oxide as Electrode for High Performance Supercapacitor. *Synth. Met.* **2016**, *217*, 237−243.
(60) Wang, S.; Shen, J.; Wang, Q.; Fan, Y.; Li, L.; Zhang, K.; Yang, L.; Zhang, W.; Wang, X. High-Performance Layer-by-Layer Self-Assembly PANI/GQD-RGO/CFC Electrodes for a Flexible Solid-State Supercapacitor by a Facile Spraying Technique. *ACS Appl. Energy Mater.* **2019**, *2*, 1077−1085.
(61) Guo, C. X.; Yilmaz, G.; Chen, S.; Chen, S.; Lu, X. Hierarchical Nanocomposite Composed of Layered V 2 O 5 /PEDOT/MnO 2 Nanosheets for High-Performance Asymmetric Supercapacitors. *Nano Energy* **2015**, *12*, 76−87.
(62) Stoller, M. D.; Ruoff, R. S. Best Practice Methods for Determining an Electrode Material's Performance for Ultracapacitors. *Energy Environ. Sci.* **2010**, *3*, 1294−1301.
(63) He, H.; Zhang, L.; Guan, X.; Cheng, H.; Liu, X.; Yu, S.; Wei, J.; Ouyang, J. Biocompatible Conductive Polymers with High Conductivity and High Stretchability. *ACS Appl. Mater. Interfaces* **2019**, *11*, 26185−26193.
(64) Asplund, M.; Thaning, E.; Lundberg, J.; Sandberg-Nordqvist, A. C.; Kostyszyn, B.; Inganäs, O.; von Holst, H. Toxicity Evaluation of PEDOT/Biomolecular Composites Intended for Neural Communication Electrodes. *Biomed. Mater.* **2009**, *4*, 045009.
(65) Salomäki, M.; Ouvinen, T.; Marttila, L.; Kivelä, H.; Leiro, J.; Mäkilä, E.; Lukkari, J. Polydopamine Nanoparticles Prepared Using Redox-Active Transition Metals. *J. Phys. Chem. B* **2019**, *123*, 2513−2524.
(66) Hirata, M.; Gotou, T.; Horiuchi, S.; Fujiwara, M.; Ohba, M. Thin-Film Particles of Graphite Oxide 1. *Carbon* **2004**, *42*, 2929−2937.
(67) Damlin, P.; Suominen, M.; Heinonen, M.; Kvarnström, C. Non-Covalent Modification of Graphene Sheets in PEDOT Composite Materials by Ionic Liquids. *Carbon* **2015**, *93*, 533−543.
(68) Omelon, S. J.; Grynpas, M. D. Relationships between Polyphosphate Chemistry, Biochemistry and Apatite Biomineralization. *Chem. Rev.* **2008**, *108*, 4694−4715.
(69) Lavalle, P.; Vivet, V.; Jessel, N.; Decher, G.; Voegel, J.-C.; Mesini, P. J.; Schaaf, P. Direct Evidence for Vertical Diffusion and Exchange Processes of Polyanions and Polycations in Polyelectrolyte Multilayer Films. *Macromolecules* **2004**, *37*, 1159−1162.
(70) Qu, J.; Ouyang, L.; Kuo, C.-c.; Martin, D. C. Stiffness, Strength and Adhesion Characterization of Electrochemically Deposited Conjugated Polymer Films. *Acta Biomater.* **2016**, *31*, 114−121.
(71) Parnell, A. J.; Cadby, A. J.; Dunbar, A. D. F.; Roberts, G. L.; Plumridge, A.; Dalgliesh, R. M.; Skoda, M. W. A.; Jones, R. A. L. Physical Mechanisms Responsible for the Water-Induced Degradation of PC61BM P3HT Photovoltaic Thin Films. *J. Polym. Sci., Part B: Polym. Phys.* **2016**, *54*, 141−146.
(72) Yamada, K.; Okamoto, M.; Sakurai, M.; Suenobu, T.; Nakayama, K.-i. Solution-Processable Reduced Graphene Oxide Template Layer for Molecular Orientation Control of Organic Semiconductors. *RSC Adv.* **2019**, *9*, 32940−32945.
(73) Hassinen, J.; Kauppila, J.; Leiro, J.; Määttänen, A.; Ihalainen, P.; Peltonen, J.; Lukkari, J. Low-Cost Reduced Graphene Oxide-Based Conductometric Nitrogen Dioxide-Sensitive Sensor on Paper. *Anal. Bioanal. Chem.* **2013**, *405*, 3611−3617.
(74) Ahonen, H. J.; Lukkari, J.; Kankare, J. n- and p-Doped Poly(3,4-ethylenedioxythiophene): Two Electronically Conducting States of the Polymer. *Macromolecules* **2000**, *33*, 6787−6793.

https://dx.doi.org/10.1021/acs.langmuir.0c00824
Langmuir 2020, 36, 6736−6748

(75) Wakabayashi, T.; Katsunuma, M.; Kudo, K.; Okuzaki, H. PH-Tunable High-Performance PEDOT:PSS Aluminum Solid Electrolytic Capacitors. *ACS Appl. Energy Mater.* **2018**, *1*, 2157−2163.
(76) de Kok, M. M.; Buechel, M.; Vulto, S. I. E.; van de Weijer, P.; Meulenkamp, E. A.; de Winter, S. H. P. M.; Mank, A. J. G.; Vorstenbosch, H. J. M.; Weijtens, C. H. L.; van Elsbergen, V. Modification of PEDOT:PSS as Hole Injection Layer in Polymer LEDs. *Phys. Status Solidi A* **2004**, *201*, 1342−1359.
(77) He, S.; Mukaida, M.; Kirihara, K.; Lyu, L.; Wei, Q. Reversible Protonic Doping in Poly(3,4-Ethylenedioxythiophene). *Polymers* **2018**, *10*, 1065.
(78) Bredas, J. L.; Street, G. B. Polarons, Bipolarons, and Solitons in Conducting Polymers. *Acc. Chem. Res.* **1985**, *18*, 309−315.
(79) van Haare, J. A. E. H.; Havinga, E. E.; van Dongen, J. L. J.; Janssen, R. A. J.; Cornil, J.; Brédas, J.-L. Redox States of Long Oligothiophenes: Two Polarons on a Single Chain. *Chem.—Eur. J.* **1998**, *4*, 1509−1522.
(80) Zozoulenko, I.; Singh, A.; Singh, S. K.; Gueskine, V.; Crispin, X.; Berggren, M. Polarons, Bipolarons, And Absorption Spectroscopy of PEDOT. *ACS Appl. Polym. Mater.* **2019**, *1*, 83−94.
(81) Kauppila, J.; Kunnas, P.; Damlin, P.; Viinikanoja, A.; Kvarnström, C. Electrochemical Reduction of Graphene Oxide Films in Aqueous and Organic Solutions. *Electrochim. Acta* **2013**, *89*, 84−89.
(82) Kotov, N. A.; Dékány, I.; Fendler, J. H. Ultrathin Graphite Oxide−Polyelectrolyte Composites Prepared by Self-Assembly: Transition between Conductive and Non-Conductive States. *Adv. Mater.* **1996**, *8*, 637−641.
(83) Baba, A.; Lübben, J.; Tamada, K.; Knoll, W. Optical Properties of Ultrathin Poly(3,4-Ethylenedioxythiophene) Films at Several Doping Levels Studied by In Situ Electrochemical Surface Plasmon Resonance Spectroscopy. *Langmuir* **2003**, *19*, 9058−9064.
(84) Wijeratne, K.; Vagin, M.; Brooke, R.; Crispin, X. Poly(3,4-Ethylenedioxythiophene)-Tosylate (PEDOT-Tos) Electrodes in Thermogalvanic Cells. *J. Mater. Chem. A* **2017**, *5*, 19619−19625.
(85) Sahalianov, I.; Singh, S. K.; Tybrandt, K.; Berggren, M.; Zozoulenko, I. The Intrinsic Volumetric Capacitance of Conducting Polymers: Pseudo-Capacitors or Double-Layer Supercapacitors? *RSC Adv.* **2019**, *9*, 42498−42508.
(86) Aasmundtveit, K. E.; Samuelsen, E. J.; Pettersson, L. A. A.; Inganäs, O.; Johansson, T.; Feidenhans'l, R. Structure of Thin Films of Poly(3,4-Ethylenedioxythiophene). *Synth. Met.* **1999**, *101*, 561−564.
(87) Lee, S.; Cho, M. S.; Lee, H.; Nam, J.-D.; Lee, Y. A Facile Synthetic Route for Well Defined Multilayer Films of Graphene and PEDOTvia an Electrochemical Method. *J. Mater. Chem.* **2012**, *22*, 1899−1903.
(88) Kurra, N.; Park, J.; Alshareef, H. N. A Conducting Polymer Nucleation Scheme for Efficient Solid-State Supercapacitors on Paper. *J. Mater. Chem. A* **2014**, *2*, 17058−17065.
(89) Lee, J. E.; Park, S. J.; Kwon, O. S.; Shim, H. W.; Jang, J.; Yoon, H. Systematic Investigation on Charge Storage Behaviour of Multidimensional Poly(3,4-Ethylenedioxythiophene) Nanostructures. *RSC Adv.* **2014**, *4*, 37529−37535.
(90) Fong, K. D.; Wang, T.; Kim, H.-K.; Kumar, R. V.; Smoukov, S. K. Semi-Interpenetrating Polymer Networks for Enhanced Supercapacitor Electrodes. *ACS Energy Lett.* **2017**, *2*, 2014−2020.
(91) Snook, G. A.; Chen, G. Z. The Measurement of Specific Capacitances of Conducting Polymers Using the Quartz Crystal Microbalance. *J. Electroanal. Chem.* **2008**, *612*, 140−146.

https://dx.doi.org/10.1021/acs.langmuir.0c00824
Langmuir 2020, 36, 6736−6748